COMMUNICATION

Unraveling a two-step oxidation mechanism in electrochemical Cu-MOF synthesis†

Philipp Schäfer,[a] Monique A. van der Veen*[b] and Katrin F. Domke*[a]

To employ the full potential of electrochemical (ec) synthesis to grow metal–organic frameworks (MOFs) in more complex organizations at the mesoscale, it is vital to understand the underlying crystallization reaction pathway. For the MOF most typically grown electrochemically, CuBTC, we systematically investigated the role of oxygen species in the synthesis.

Metal–organic frameworks (MOFs) attract significant interest as versatile materials for gas separation[1] and storage,[2] and more recently as light harvesters for novel energy conversion schemes.[3,4] Their topology (crystal structure, pore size, pore connectivity) and functionality (chemistry at reactive sites, luminescence/absorption properties of framework, guest donor/acceptor moieties) can, in principle, be tuned to desire by making use of the wealth of metal ion and organic linker combinations the chemist's tool kit provides. While classically, MOFs are synthesized solvothermally at elevated pressure and/or temperature,[5,6] recently, novel anodic and cathodic[7–12] electrochemical (ec) fabrication protocols are emerging as electrosynthesis offers milder conditions, greater energy efficiency and energetic control over the MOF growth.[7,13,14]

It has been shown that by applying an appropriate synthesis potential, the size of MOF crystals can be directly controlled in the sub- to 5 μm size range,[7,8] or that different linkers can be built in on demand to fabricate multi-functionality MOFs *in situ*.[10] These cases demonstrate the extraordinary possibilities electrosynthesis offers for controlled MOF growth. However, generalizing the ec approach requires a detailed understanding of the underlying reaction mechanisms which have to date only been speculated on.[7,15] Questions regarding the chemical species involved, the role of the substrate surface and the energetics and

kinetics of the overall reaction pathway of ec MOF formation need to be answered to mature ec synthesis into a readily available tool for rational MOF design.

In this work, we unravel the reaction mechanism of the ec formation of a showcase MOF, CuBTC (HKUST-1; Cu 1,3,5 tricarboxylic acid). Prepared according to the original protocol from 2005, electrosynthesized CuBTC, finds large-scale application *e.g.* for carbon dioxide/methane[16] or propylene/propane[17] gas mixture separation, or in novel sensors and electronic devices.[18] Despite CuBTC being one of the most extensively studied MOFs,[7,19] its ec formation mechanism has not yet been unraveled, hindering full exploitation of electrosynthetic MOF design possibilities. It has been postulated that, Cu is anodically oxidized in one step to Cu^{2+} followed by linker coordination in solution.[7,15] Other groups, however, have observed MOF crystals intergrown with the surface that suggest on-surface growth.[20]

To solve the prevailing controversy and open a route for rational MOF topology and functionality design, we set out to identify the chemical species involved in CuBTC electro-synthesis and unravel the reaction mechanism. We systematically varied the experimental conditions such as the Cu source, the presence of O_2 and the applied potential (Table 1), generally following the protocol found in literature:[7,21] a Cu plate was immersed at open circuit in a mixture of 100 mL absolute EtOH, 3 g BTC linker and

[a] *Max Planck Institute for Polymer Research, Molecular Spectroscopy Department, Ackermannweg 10, D 55128 Mainz, Germany. E-mail: domke@mpip-mainz.mpg.de*
[b] *Delft University of Technology, Faculty of Applied Sciences, Chemical Engineering Department, Section of Catalysis Engineering, Julianalaan 136, NL 2628 BL Delft, Netherlands. E-mail: M.A.vanderVeen@tudelft.nl*

† Electronic supplementary information (ESI) available: Materials and methods (Raman, XRD, SEM data); characterization of Samples F. Current transients. See DOI: 10.1039/c6cc00534a

Table 1 Experimental conditions, sample overview

Sample type	Cu source	O_2 presence	E^a/reaction time	CuBTC formation
A	Cu with natural oxide layer	Yes	1 V/20 min	Yes
B	Cu, oxide free	No	1 V/20 min	No
C	Cu with artificial oxide layer	No	1 V/20 min	Yes
D	Cu_2O	Yes	No/16 hours	Yes
E	Cu_2O	Low amount	No/16 hours	Yes (truncated)
F[b]	CuO	Yes	No/16 hours	No

[a] Potentials reported *vs.* Ag/AgCl/3 M KCl. [b] SEM/Raman characterization in ESI.

1 g methyl tributyl ammonium methyl sulfate electrolyte. After electrode immersion, a potential of $E = 1$ V vs. Ag/AgCl was applied for 20 min. To prevent Cu_2O formation on the Cu electrode from ambient aerobic corrosion in O_2-free experiments, EtOH was degassed with Ar for 20 min prior to Cu immersion, and the ec cell was constantly kept under Ar. To remove the natural oxide layer (comprised mainly of Cu_2O and a small amount of CuO and $Cu(OH)_2$[22]), the Cu electrode was etched with 25% HNO_3 and 25% HCl[23] before transfer to the synthesis cell.

The resulting topography and chemical composition of each sample type was characterized to determine whether CuBTC grows under the respective conditions. CuBTC is known to form octahedral crystals that can be seen with scanning electron microscopy (SEM).[24] Raman in-plane ring bending vibrations at 743 and 825 cm^{-1} of the BTC moiety in CuBTC confirm the presence of CuBTC (Fig. S2 and Table S1, ESI†).[25] X-ray diffraction (XRD) was used for CuBTC identification where a sufficient amount of MOF crystals was obtained (see ESI,† for experimental details).

Fig. 1 shows the SEM and Raman results for the different sample types under investigation. Samples A were fabricated under synthesis conditions similar to the ec synthesis protocols found in literature,[7,21] i.e. starting from a Cu-electrode with a natural oxide layer and taking no precautions to avoid the presence of O_2. As expected, octahedral crystals of CuBTC of <1 μm to 5 μm in diameter form (Fig. 1A). Electrode coverage is incomplete at ∼20 particles per 100 $μm^2$, likely due to the low potential of 1 V. An increased synthesis time should improve surface coverage. The corresponding Raman spectrum in the inset of Fig. 1A displays the characteristic bending vibrations of CuBTC at 743 and 825 cm^{-1}, and XRD diffractograms confirm the successful synthesis of CuBTC (Fig. S1A, ESI†). Note that the Raman spectrum also shows a significant contribution of Cu_2O (see Fig. S3A, ESI,† broad peaks at 525 and 626 cm^{-1}).

Samples B were produced under oxide- and O_2-free conditions, thus void of all components unnecessary for the Cu^{2+} dissolution-coordination mechanism proposed in literature. The SEM image (Fig. 1B) shows parallel Cu tracks due to the acidic etching of the surface. With exception of only about 1 particle per 100 $μm^2$ of ca. 0.5 to 1 μm diameter, no CuBTC crystals are visible. The CuBTC response in the Raman spectra can hardly be distinguished from the noise (Fig. 1B inset), and no XRD signal of CuBTC was obtained (Fig. S1B, ESI†).

To find the smallest set of components required to enable CuBTC synthesis, we electrochemically oxidized the surface of the Cu plate on purpose by immersing it in the electrolyte solution and applying a potential of 1 V vs. Ag/AgCl for 25 min prior to O_2-free MOF synthesis (Samples C). SEM, Raman and XRD confirm the successful synthesis of CuBTC (Fig. 1C and Fig. S1C, ESI†); the Raman spectrum shows a significant Cu_2O contribution (Fig. S3C, ESI†). Samples C are covered with a mixture of about 5 crystals per 100 $μm^2$ of octahedral crystals of 3 to 5 μm diameter and ca. 50 particles per 100 $μm^2$ in the sub-μm diameter range. At some spots, the smaller crystals cover the larger particles.

From experiments A to C, we learn that oxygen plays an important role in ec CuBTC synthesis as CuBTC crystals do not grow under O_2-oxygen free conditions and Cu_2O is always present on the electrodes. To further investigate the role of oxygen, we used pure oxides as precursors for CuBTC growth. For Samples D, we immersed Cu_2O powder in an ethanolic solution of 0.15 M BTC without any other additions for 14 hrs under ambient conditions. No potential was applied. A blue powder was isolated by centrifugation and characterized. The SEM micrograph in Fig. 1D shows octahedral crystals of 1 to 5 μm diameter that are intergrown into larger agglomerates of 10 to 15 μm length. Raman spectra (Fig. 1D inset) and XRD (Fig. S1D, ESI†) confirm CuBTC synthesis. Interestingly, an analogous experiment with CuO powder as starting material did not produce any CuBTC (Samples F, ESI†).

To identify the necessary oxidation agent for the oxidation of Cu(I) to Cu(II) in absence of an applied potential, Samples E were synthesized like Samples D, but in an O_2-deficient environment. The solution was degassed for 15 min, but during transfer into a glove box, some O_2 could re-dissolve. The SEM micrographs show about 10% of the Cu_2O surface covered with octahedral crystals of diameters between 0.3 and 0.7 μm,
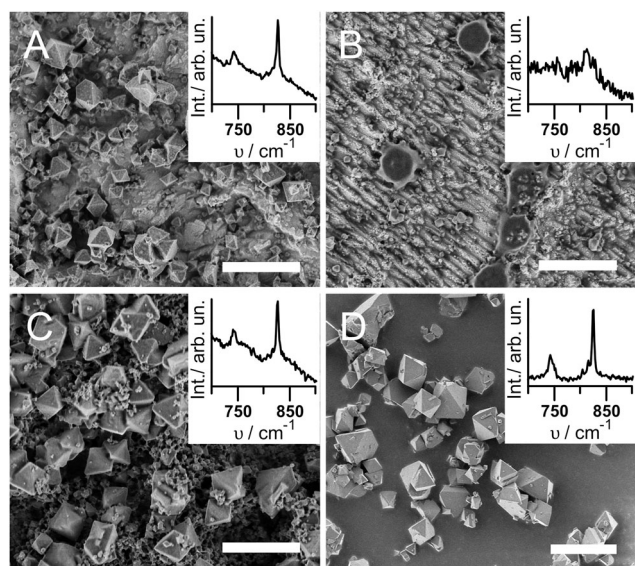

Fig. 1 SEM micrographs and Raman spectra of Samples A to D. Scale bar: 10 μm.

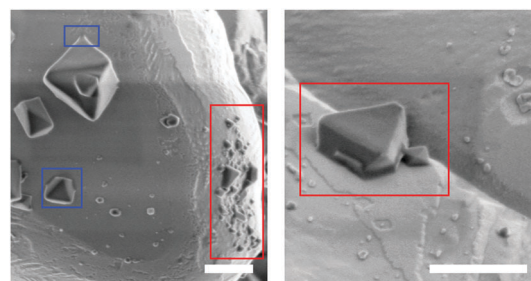Fig. 2 SEM of Samples E. Red: truncated crystals; blue: intergrowth with surface. Scale bar: 500 nm.

and partly with what seem to be incomplete CuBTC crystals with diameters of 100 to 200 nm (Fig. 2, red). This is the only Sample for which we observe incomplete CuBTC octahedrons. It is unlikely that these crystals deposited onto the Cu_2O substrate during centrifugation; rather they must have grown at the surface, and their growth was halted prematurely due to lack of O_2. Similarly, also the few octahedral crystals (Fig. 2, blue) are visibly attached to the Cu_2O substrate. From these results, we conclude that O_2 is the necessary oxidant for the oxidation of Cu_2O to CuBTC without ec potential. Furthermore, the visible connection between the CuBTC and the Cu_2O indicates that CuBTC nucleation likely takes place directly at the Cu_2O solid/liquid interface. Summing up, the first step to ec CuBTC formation is the oxidation of Cu to Cu^{1+} achieved either by ec oxidation of the Cu anode or by providing O_2 and/or H_2O (H_2O enables CuBTC synthesis even under inert conditions.[20]) as reactant. Cu_2O is the predominant oxidation product of Cu in ethanol.[26] Note that also $Cu(OH)_2$ readily converts into CuBTC in presence of the linker.[27] While $Cu(OH)_2$ as an inter-mittent, short-lived reaction intermediate cannot be excluded, our spectroscopic data does not indicate stable $Cu(OH)_2$ formation (i.e. no Raman band at 460 cm^{-1}, Fig. S2b, ESI†). Furthermore, CuBTC forms directly from Cu^{1+}_2O powder while $Cu^{2+}O$ does not convert to CuBTC under the given experimental conditions.

As known from literature, Cu_2O can be produced from Cu by the following oxidation reactions with H_2O or O_2:[22,28]

$$2Cu + H_2O \leftrightarrow Cu_2O + 2H^+ + 2e^- \qquad (1)$$

$$4Cu + O_2 \leftrightarrow 2Cu_2O \qquad (2)$$
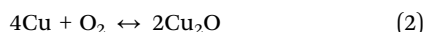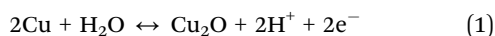
A positive applied potential facilitates the net release of electrons in reaction (1). Excess electrons are transferred to the counter electrode where a not-further specified counter reaction takes place. Reaction (2) represents the aerobic oxidation of Cu that takes place in the presence of O_2. In Samples B, both (1) and (2) were blocked by using dry EtOH and by degassing the electrolyte with Ar. Since all surface oxides were removed by acidic etching, no Cu_2O – and thus no CuBTC – could be formed.

Instead of using O_2 or H_2O as oxidant, Cu can be electro-chemically oxidized. In absence of O_2 and H_2O, the amount of available Cu^{+1}_2O is expected to limit the CuBTC yield. Indeed, for Samples C, we did not observe continuous detachment of large MOF crystals from the electrode into the solution phase, indicating that CuBTC growth stopped after all provided Cu_2O had been consumed.

For the second oxidation step of Cu^{1+}_2O to $Cu^{2+}BTC$, we propose the following ec half reaction:

$$3Cu_2O + 4H_3BTC \leftrightarrow 2Cu_3BTC_2 + 3H_2O + 6e^- + 6H^+ \qquad (3)$$

H_2O is a likely product that can be produced from the oxygen released from Cu_2O and the protons released from BTC. In the ec synthesis, this oxidation half-reaction takes place at the Cu anode. (A corresponding, not further specified reduction reac-tion takes place at the counter electrode.) With the production

of H_2O, the reaction should be self-sustaining after a certain threshold H_2O concentration is reached. For aerobic Cu_2O oxidation (Samples D), CuBTC growth occurs at the Cu_2O/ solution interface. CuBTC synthesis from Cu_2O without applied potential is only possible in the presence of O_2, as shown by the greatly reduced amount of CuBTC in Samples E. Likely, O_2 is reduced to H_2O in a counter reaction

$$O_2 + 4H^+ + 4e^- \leftrightarrow 2H_2O \qquad (4)$$
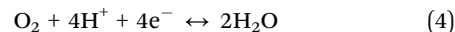
Eqn (3) as the key step in ec CuBTC synthesis as derived from our results is fully consistent with synthesis facts reported in literature: Van Assche et al. showed that CuBTC cannot be produced electrochemically in electrolytes that contain more than 50% H_2O.[20] The suppression of the reaction by H_2O is consistent with H_2O formation on the product side of (3), leading to an increase of the oxidation potential of the reaction while increasing the propensity for the formation of H_2O-containing catena-triaqua-μ-CuBTC.[20]

Direct oxidation of solid Cu_2O to CuBTC at the ec solid/ liquid interface to start crystal nucleation likely explains the tight attachment of CuBTC crystals to the electrode as previously observed[7] as well as the incomplete CuBTC crystals visibly bound to Cu_2O that we observe under oxygen-limited conditions; however, a dissolution process with Cu_2O as intermittent cannot be completely excluded. It remains unclear whether further crystal growth happens at the Cu_2O–CuBTC–electrolyte interface or continues through a solution-based process with Cu^{2+} ions attaching to the outer facets of the growing crystal. Campagnol et al. show that electrosynthesized Cu isonicotinate grows at the MOF–electrolyte interface.[29] The significant amount of water (50%)[30] that makes Cu^{2+} ions more soluble in the form of $[Cu(H_2O)_6]^{2+}$ could explain a solution-based process. The lack of H_2O in our system, however, makes a direct comparison difficult.

Let us summarize the reaction mechanism for the ec oxidation of Cu^0 to CuBTC: in presence of O_2 and/or H_2O, Cu is oxidized in a one-electron step to Cu_2O. A second oxidation step from Cu^{1+} to Cu^{2+} in the presence of BTC directly converts Cu_2O to CuBTC. Involvement of an intermediate Cu(ı) reaction step has not been proposed so far and opens up new pathways to increase control of the synthesis.

Our newly gained knowledge that CuBTC crystallization proceeds through Cu_2O formation allows us to suggest a novel method to fabricate patterned MOF devices (Fig. 3A). As a proof of principle, we prepared a Cu substrate with both Cu and Cu_2O present by ec oxidizing the surface in the presence of NaOH.[31] Then, we selectively removed Cu_2O in a spot of ~ 1 cm diameter in the centre of the sample by pipetting a drop of 10% HCl. After removal of that drop and subsequent rinsing with EtOH, the Cu plate was covered with Cu_2O except for the acid-etched blank Cu area. Under synthesis conditions B (O_2 exclusion, 1 V), CuBTC was grown solely on the oxide-covered part of the sample as discernible in the white-light image (Fig. 3B). The left part of the image where surface oxides were removed by acidic etching shows the pristine Cu surface. To the right of the image, outside the area of the acid droplet, CuBTC has visibly grown and is spectroscopically detectable. Raman band integration
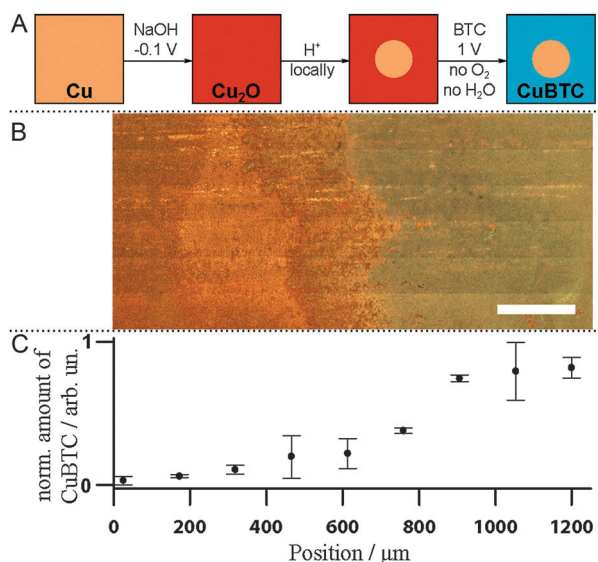
Fig. 3   A: Scheme for the fabrication of patterned CuBTC devices by oxide patterning; B: light-microscopy image of a Cu sample (left) partly covered with CuBTC (right). Scale bar: 200 μm; C: normalized amount of CuBTC across sample.

of the 800 to 850 cm^{-1} region provides the relative amounts of CuBTC at different sample positions (Fig. 3C; error bars are standard errors of the mean of three measurements taken at roughly the top, middle and bottom of the white-light image). This facile oxide-based pre-patterning approach can serve as starting point to develop improved synthesis protocols for CuBTC patterning. Current patterning approaches require the use of Cu electrodes in the desired shape (*i.e.* printed circuit boards[8] or Cu meshes[20]). Our approach offers the possibility to subsequently activate parts of a Cu substrate. It is easy to imagine how established ways to deposit Cu_2O as nanoparticles or films[32,33] or to selectively remove Cu oxide, as shown here, can be converted into a versatile basis for the fabrication of arbitrarily patterned surfaces on nm to mm length scales to create devices covered with MOF of controlled sizes at predetermined spots.

To conclude, we unravelled CuBTC electrosynthesis to proceed in a two-step oxidation mechanism at the electrode surface: Cu is first oxidized to Cu^{1+}_2O in the presence of H_2O or O_2. Cu_2O is further oxidized to $Cu^{2+}BTC$ in presence of the linker at the cuprite–electrolyte interface. The MOF octahedrons nucleate directly at the electrode surface and not in solution, rendering the ec mechanism different from the one of solvothermal syntheses with metal salts.[34,35] We demonstrate how the gained knowledge can be used for a novel quick and versatile approach to produce patterned CuBTC devices.

Notes and references

1 J. Teufel, H. Oh, M. Hirscher, M. Wahiduzzaman, L. Zhechkov, A. Kuc, T. Heine, D. Denysenko and D. Volkmer, *Adv. Mater.*, 2013, **25**, 635–639.
2 A. U. Czaja, N. Trukhan and U. Müller, *Chem. Soc. Rev.*, 2009, **38**, 1284–1293.
3 X. Zhang, W. Wang, Z. Hu, G. Wang and K. Uvdal, *Coord. Chem. Rev.*, 2015, **284**, 206–235.
4 M. A. Nasalevich, M. van der Veen, F. Kapteijn and J. Gascon, *CrystEngComm*, 2014, **16**, 4919.
5 M. G. Goesten, F. Kapteijn and J. Gascon, *CrystEngComm*, 2013, **15**, 9249.
6 Y.-R. Lee, J. Kim and W.-S. Ahn, *Korean J. Chem. Eng.*, 2013, **30**, 1667–1680.
7 A. Martinez Joaristi, J. Juan-Alcañiz, P. Serra-Crespo, F. Kapteijn and J. Gascon, *Cryst. Growth Des.*, 2012, **12**, 3489–3498.
8 R. Ameloot, L. Stappers, J. Fransaer, L. Alaerts, B. F. Sels and D. E. De Vos, *Chem. Mater.*, 2009, **21**, 2580–2582.
9 I. Hod, W. Bury, D. M. Karlin, P. Deria, C. W. Kung, M. J. Katz, M. So, B. Klahr, D. N. Jin, Y. W. Chung, T. W. Odom, O. K. Farha and J. T. Hupp, *Adv. Mater.*, 2014, **26**, 6295–6300.
10 M. Li and M. Dincă, *Chem. Sci.*, 2014, **5**, 107.
11 M. Li and M. Dincă, *Chem. Mater.*, 2015, **27**, 3203–3206.
12 I. Stassen, M. Styles, T. R. C. Van Assche, N. Campagnol, J. Fransaer, J. F. M. Denayer, J. C. Tan, P. Falcaro, D. E. De Vos and R. Ameloot, *Chem. Mater.*, 2015, **27**, 1801–1807.
13 N. Campagnol, T. R. C. Van Assche, T. Boudewijns, J. F. M. Denayer, K. Binnemans, D. E. De Vos and J. Fransaer, *J. Mater. Chem. A*, 2013, **1**, 5827.
14 M. Li and M. Dincă, *J. Am. Chem. Soc.*, 2011, **133**, 12926–12929.
15 H. Al-Kutubi, J. Gascon, E. J. R. Sudhölter and L. Rassaei, *ChemElectroChem*, 2015, **2**, 462–474.
16 T. Asadi, M. R. Ehsani, A. M. Ribeiro, J. M. Loureiro and A. E. Rodrigues, *Chem. Eng. Technol.*, 2013, **36**, 1231–1239.
17 J.-W. Yoon, I.-T. Jang, K.-Y. Lee, Y.-K. Hwang and J.-S. Chang, *Bull. Korean Chem. Soc.*, 2010, **31**, 220–223.
18 J. Gascon and F. Kapteijn, *Angew. Chem., Int. Ed.*, 2010, **49**, 1530–1532.
19 B. Panella, M. Hirscher, H. Pütter and U. Müller, *Adv. Funct. Mater.*, 2006, **16**, 520–524.
20 T. R. C. Van Assche, G. Desmet, R. Ameloot, D. E. De Vos, H. Terryn and J. F. M. Denayer, *Microporous Mesoporous Mater.*, 2012, **158**, 209–213.
21 T. R. C. Van Assche and J. F. M. Denayer, *Chem. Eng. Sci.*, 2013, **95**, 65–72.
22 I. Platzman, R. Brener, H. Haick and R. Tannenbaum, *J. Phys. Chem. C*, 2008, **112**, 1101–1108.
23 L. C. Hall, C. P. Major, J. J. Steppan, J. A. Roth and B. K. Vaughen, *J. Electrochem. Soc.*, 1987, **134**, 1902.
24 Q. Min Wang, D. Shen, M. Bülow, M. Ling Lau, S. Deng, F. R. Fitch, N. O. Lemcoff and J. Semanscin, *Microporous Mesoporous Mater.*, 2002, **55**, 217–230.
25 C. Prestipino, L. Regli, J. G. Vitillo, F. Bonino, a. Damin, C. Lamberti, a. Zecchina, P. L. Solari, K. O. Kongshaug and S. Bordiga, *Chem. Mater.*, 2006, **18**, 1337–1346.
26 B. Stypuła, J. Banaś, M. Starowicz, H. Krawiec, A. Bernasik and A. Janas, *J. Appl. Electrochem.*, 2006, **36**, 1407–1414.
27 G. Majano and J. Perez-Ramirez, *Adv. Mater.*, 2013, **25**, 1052–1057.
28 H. Y. H. Chan, C. G. Takoudis and M. J. Weaver, *J. Phys. Chem. B*, 1999, **103**, 357–365.
29 N. Campagnol, T. R. C. Van Assche, L. Stappers, J. F. M. Denayer, K. Binnemans, D. E. De Vos and J. Fransaer, *ECS Trans.*, 2014, **61**, 25–40.
30 B. Van de Voorde, R. Ameloot, I. Stassen, M. Everaert, D. E. De Vos and J.-C. Tan, *J. Mater. Chem. C*, 2013, **1**, 7716.
31 J. C. Hamilton, J. C. Farmer and R. J. Anderson, *J. Electrochem. Soc.*, 1986, **133**, 739.
32 P. E. de Jongh, D. Vanmaekelbergh, J. J. Kelly and P. E. D. Jongh, *Chem. Mater.*, 1999, **11**, 3512–3517.
33 D. P. Singh, N. R. Neti, A. S. K. Sinha and O. N. Srivastava, *J. Phys. Chem. C*, 2007, **111**, 1638–1645.
34 V. Stavila, J. Volponi, A. M. Katzenmeyer, M. C. Dixon and M. D. Allendorf, *Chem. Sci.*, 2012, **3**, 1531.
35 O. Shekhah, H. Wang, D. Zacher, R. A. Fischer and C. Wöll, *Angew. Chem., Int. Ed.*, 2009, **48**, 5038–5041.